Surface & Coatings Technology 357 (2019) 289–303

Contents lists available at ScienceDirect

Surface & Coatings Technology

journal homepage: www.elsevier.com/locate/surfcoat

Multi-variable optimisation of the quality characteristics of fiber-laser cladded Inconel-625 composite coatings

E.O. Olakanmi[a,*], S.T. Nyadongo[a], K. Malikongwa[a], S.A. Lawal[b], A. Botes[c], S.L. Pityana[d]

[a] Botswana International University of Science & Technology, Palapye, Botswana
[b] Federal University of Technology, Minna, Nigeria
[c] Materials Science Manufacturing, Council for Scientific & Industrial Research, Pretoria, South Africa
[d] Laser Enabled Manufacturing, NLC, Council for Scientific & Industrial Research, Pretoria, South Africa

ARTICLE INFO

Keywords:
Response surface modeling (RSM)
Inconel 625/WC composite
Process efficiency
Dilution ratio
Optimisation
Energy density

ABSTRACT

Inappropriate choice of processing and materials parameters when re-manufacturing industrial equipment, via laser cladding (LC) technique, has adverse implications for attaining durability of equipment in terms of functional performance, efficient lead time and cost savings for equipment repairers. In an attempt to promote the adoption of LC as an efficient equipment re-manufacturing process, this study employs central composite design (CCD) and response surface modeling (RSM) to build mathematical models for optimising the quality characteristics (dilution ratio and microhardness and LC process efficiency) of a composite coating. The quality characteristics of the coating, comprising of Inconel 625 matrix reinforced with tungsten carbide (WC) particles, were optimised as functions of laser energy density, inconel content in the composite coating and shielding gas flow rates. Evidence from this study establishes that laser energy density is the dominant factor which influences all the output responses. It was also revealed that predicted values of the quality characteristics agree with the experimental results within the permissible range of the LC process and materials variables. Consequently, dilution ratio was minimised as coating's microhardness and process efficiency were maximised with appropriate combination of laser energy density, inconel content and shielding gas flow rates. Finally, it may be inferred from this analysis that quality characteristics are optimised at 67.6 wt% inconel content, laser energy density (18.60 J/mm^2) and career/shielding gas flow rates (8.86 l/min) with desirability value of 1.00.

1. Introduction

Gas turbine parts used in power generation sector do encounter high temperature oxidation, corrosion and wear due to their severe operating environments. Inconel 625 alloy, having high corrosion and oxidation resistance property, has been widely employed in re-manufacturing gas turbine components when they suffer structural damage in order to prolong their service life. This alloy contains nickel and chromium matrix of which its metallurgical reactions with molybdenum and niobium provides stiffness and moderate strength. Meanwhile, to improve the wear performance of Inconel 625 when employed in repairing gas turbine components, it is required that it is reinforced with appropriate structural materials characterised with high erosion resistance. It had been reported that cermets impart excellent high temperature wear and erosion resistance when incorporated into Inconel 625 matrix [1–3]. Hence, the suitability of Inconel 625/WC composite coating for industrial application such as gas turbine parts in which challenges of corrosion and erosion are highly prevalent [4,5].

Among the techniques for repairing engineering components are tungsten inert gas (TIG) welding, high velocity oxy-fuel (HVOF), plasma spraying (PS) and laser cladding (LC). LC, a sub-set of laser material processing (LMP) techniques, offers unique advantages such as limited heat-affected zone, smaller stress deformation, lower dilution rate and good metallurgical bonding between the coating and the substrate [6,7] over vacuum plasma spray and HVOF techniques which are associated with processing challenges such as component distortion, undesirable intermetallic phases, poor mechanical properties and higher residual stresses during processing [8]. For instance, Tuominen et al. [9] compared electrochemical performance of Inconel 625 coatings deposited by HVOF and laser cladding techniques in de-aerated 3.5 wt% NaCl solution. The outcome of the study revealed that LC deposited coating exhibited improved corrosion resistance in terms of lower passive current density, higher break-down potential and corrosion potential

* Corresponding author.
E-mail address: olakanmie@biust.ac.bw (E.O. Olakanmi).

https://doi.org/10.1016/j.surfcoat.2018.09.063
Received 18 June 2018; Received in revised form 21 September 2018; Accepted 26 September 2018
Available online 26 September 2018
0257-8972/

while the inferior corrosion resistance of HVOF coating was attributed to inhomogeneous coating structure resulting from porosity and oxide formation alongside the presence of inter-connected paths which were absent in the LC deposited coating. Sexton and co-investigators [10] also assessed the microstructure, hardness, cracking, porosity and dilution rate of LC deposited Inconel 625 coatings on Inconel 713 substrate and established that the use of LC in repairing nickel based super alloy is more beneficial relative to the tungsten inert gas welding (TIG) welding technique.

Analysis of available literature on the LC of Inconel 625 and its composite coatings [1–7,11–15] suggests that corrosion, microstructure and mechanical properties are the most studied output variables. The effects of process parameters such as laser power, feed rate, scanning speed and laser beam spot size on these output variables are well explored. Meanwhile, these studies had not considered laser energy density; an important parameter which consolidates the effects of laser power (P), scanning velocity (V) and beam diameter (d) with a view to providing insightful understanding of how heat dissipation in LC process influences the solidification mechanism and the development of quality characteristics of coatings. It may then be inferred that available studies have not provided a holistic understanding of how heat transfer influence consolidation mechanism in LC process. This is because the studies only considered the effects of laser power, scanning velocity and beam diameter on one-by-one basis. Hence, this study addresses this missing gap in our understanding of how the consolidated LC parameter known as energy density alongside inconel 625 content in the composite coating and shielding gas flow-rates influence the solidification phenomenon and the development of the quality characteristics of the coatings.

Furthermore, experimental work in the referred studies was carried out via one-by-one variable experimental design. A major demerit of the one-by-one variable experimental design is that it does not allow for appropriate parameter combination for optimising the quality characteristics of the coatings. Response surface modeling (RSM), a statistical technique, has been engaged for exploring the relationships between the quality characteristics of various manufacturing processes and their independent variables [16–21]. This is due to the fact that it is capable of predicting the quality characteristics via the selection of appropriate multi-parametric combination [22]. In this paper, response surface modeling (RSM) technique is employed via the design of experiments (DOE) to establish the effects of variation in laser energy density, inconel content in the composite coating and shielding gas flow rate on (i) microhardness (ii) dilution ratio (iii) deposition/process efficiency and (iv) microstructure for multi-track, multi-layer laser-cladded Inconel 625/WC composite coating on 304L stainless steel. Microhardness and dilution ratio are selected as quality characteristics of the composite coatings because appropriate laser-materials interaction in designing coatings characterised with minimal dilution which imparts optimum microhardness must be established. No less important is also the materials' formulation to achieve these goals while sustaining the coating manufacturing business profitably. Therefore, the objective of this study is to optimise the process parameters for attaining appropriate solidification mechanism which strongly influence the track geometry for attaining high process efficiency and microhardness as well as minimum dilution ratio.

2. Experimental design and the method of analysis

The range of process parameters used in this work were determined via preliminary studies and these were subsequently confirmed by discussion with industrial experts at the Laser Enabled Manufacturing (LEM) research group at the Council for Scientific and Industrial Research (CSIR), Pretoria, South Africa as well as consultation with relevant literature [23]. All the variable parameters (energy density, Inconel content in the composite coating and shielding gas flow rate) were limited within a design domain whereas the stand-off distance (12 mm) and overlapping ratio (50%) were kept constant. Energy density, ED (J/mm^2) is defined as shown in Eq. (1)

Table 1
Selected process parameters used in this study.

Parameters	Energy density (J/mm^2)	Component ratio In:WC-86 (rev/min)	Carrier/shielding gas flow rate (l/min)
Designations	A	B	C
High alpha level (1.6818)	24.8 (2272 W)	(2.6) 96.7:3.3 (0.1)	14.72
High level (1)	21.9 (2000 W)	(2.1) 90:10 (0.5)	12.0
Zero level (0)	17.5 (1600 W)	(1.9) 80:20 (1.1)	8.0
Low level (−1)	13.1 (1200 W)	(1.6) 70:30 (1.8)	4.0
Low alpha level (−1.6818)	10.1 (928 W)	(1.5) 63.3:36.7 (2.2)	1.28
Variation range Δ_i	4.4	10.0	4.0

$$\text{Energy density (ED)} = P/(V*d) \quad (1)$$

where P (1200 to 2000 W) is the power, V (25 mm/s) is the scanning velocity and d (4 mm) is the beam diameter. Eq. (1) presents the energy density (J/mm^2) which consolidates the laser processing conditions for fabricating the multiple tracks, multiple-layer of Inconel 625/WC coatings using the fiber laser.

Central composite design (CCD) was used to analyse the effects of change in parameters using Design Expert 7 software. Each independent process variable was varied and coded to high alpha level, high level, zero level, low level and low alpha level as shown in Table 1. The CCD employs 20 runs of experiments which include 6 central experimental points and 14 axial points with a view to optimising the quality characteristics of the of the Inconel 625/WC composite coatings by analysing the process parameters and the measured quality characteristics. The measured responses obtained from this study included microhardness (MH), height of the cladding track (H), molten depth of the substrate (h), mass of the constituent powders deposited with (m) and without (M) laser beam. Data for m and M were measured for a period of 4 min for which it took each clad to be deposited for each experimental condition. The molten depth of the substrate (h) and the height of the clad track (H) were used in computing the dilution ratio (DR) as shown in Eq. (2). Fig. 1 shows how dilution ratio (DR) was determined through the measurement of h (molten depth of the substrate in μm) and H (height of the clad in μm). Process efficiency (PE) was determined by Eq. (3) according to Lee [24]. PE measures the productivity of the laser cladding system by comparing the input resource (M) to the output product (m) (which is the mass of the powder input and the mass of the final clad). PE enables the amount of powder loss during LC processing of the composite coatings to be evaluated and minimised. Hence, the quality characteristics namely microhardness (MH), dilution ratio (DR) and process efficiency (PE) constituted the output value of the developed mathematical model.

$$\text{Dilution ratio (DR)} = h/(h + H) \quad (2)$$

$$\text{Process Efficiency (PE)} = m/M \quad (3)$$

RSM engages multiple regression statistical technique to build the empirical models in analysing the relationship between the process parameters and the quality characteristics of the coatings. In this study, the second order regression associated with the polynomial expression in Eq. (4) was engaged.

$$y = \beta_o + \sum_{j=1}^{k} \beta_j X_j + \sum_{j=1}^{k} \beta_{jj} X_j^2 + \sum_{i<j} \sum_{j=2}^{k} \beta_{ij} X_i X_j + \varepsilon \quad (4)$$

where y is the predicted response, β_o is a constant, β_j is the jth linear coefficient, β_{jj} is the jth quadratic coefficient, β_{ij} is the ith interaction coefficient, X_j is the independent variable, k is the number of factors and ε is the residual error. Furthermore, coefficients of the models were

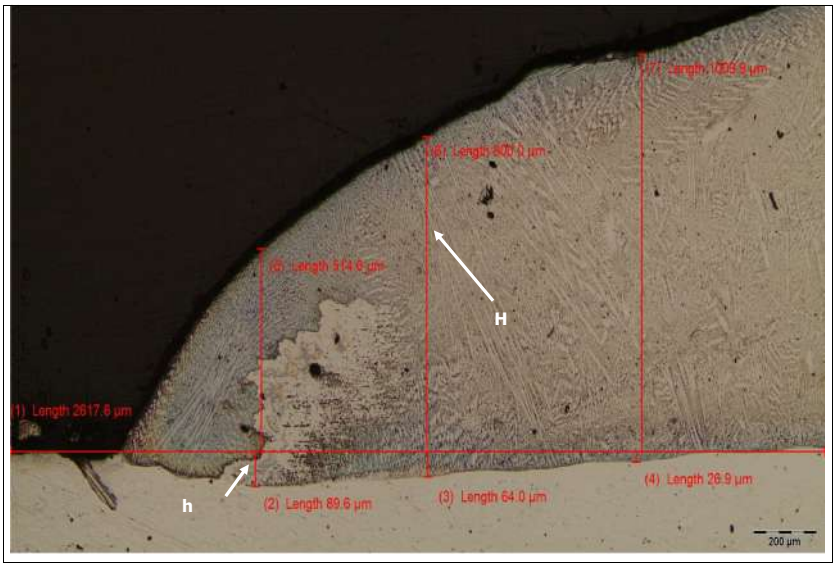

Fig. 1. A micrograph showing the determination of dilution ratio (DR) through the measurement of h (molten depth of the substrate in µm) and H (height of the clad in µm).

predicted via regression analysis based on two groups of twenty measured responses.

3. Experimental procedure

The substrate material used in this experimental work was stainless steel AISI 304L while the powdered materials (Inconel 625 and tungsten carbide WC-86) were supplied by Kennametal SA (PTY) LTD. The composition in weight (wt%) of inconel 625 powder is presented in Table 2 with standard deviation of ± 5%. This was determined by energy dispersive spectroscopy (EDS). The composite coating was deposited on a 304L stainless steel substrate machined to dimensions of 100 mm × 50 mm × 10 mm. Prior to deposition, acetone was used to clean the substrate steel plate in order to remove any impurity on the surface and improve adhesion of the deposited clad. The clad material consists of varying proportions of inconel 625 (Fig. 2a) and tungsten carbide (WC-86) (Fig. 2b) powders of particle size distribution 45–90 µm and 38–75 µm respectively. Both powders have spherical morphology as seen in Fig. 2a and b.

The laser cladding was conducted using an IPG YLS 5000 Fibre Laser system having maximum power of 5 kW and wavelength of 1.064 µm. The laser system shown in Fig. 3, is located at the Council of scientific and industrial research (CSIR), Pretoria, South Africa. A 3-way coaxial nozzle system was connected to a 5-axis CNC machine and a multi-hopper powder feed system to the nozzle. Argon was used as shielding and carrier gas at varying flow rates (Table 1). This study employed DPSF-D3 powder feed system. The allowable range of powder particle size it can feed varies from 20 to 200 µm while it has three cylinders with a feed rate deviation of 2%. Meanwhile, it controls the powder feed rate indirectly through its rotary speed rather than through its output mass of powder material. Flowability graphs of the powders were employed to set the feed rates of inconel 625 and WC-86. The ratio of the feed rates of the composite constituents was used in determining their component ratio for each experimental condition as indicated in Table 1. Clads made of inconel 625/WC-86 composite coating were produced in 10 tracks and four layers according to experimental matrix shown in Table 3 in random order. The cladding thickness for each sample fabricated with each process parameter was observed to be uniform over the area covered during the experiments. Each sample was replicated twice. Similar to the approach adopted by [25] while depositing aluminium coatings via laser assisted cold spray (LACS) process, cross-sections of clads (see Fig. 4) for characterisation were obtained from the middle of the clad tracks where deposition was continuous. Samples were hot press mounted in a cross-sectional view as shown by the sample preparation schematic diagram in Fig. 4. They were then grinded and polished using a Struers Cito-Press 5 mounting machine as well as a Struers grinding and polishing machine respectively.

Electro etching was carried out on the samples using a 10% oxalic acid agent at 4.95v in order to reveal the molten depth of the substrate. Observation under an optical microscope was carried out to examine each sample for height of the cladding track (H) and molten depth of the substrate (h). The microhardness (MH) of all the coating samples was measured by a Vickers hardness tester (Leitz, Germany) with a load of 0.05 N and a holding time of 10.0 s according to ASTM E92 standards. The experimental responses reported in Table 3 were the average values of at least 15 microhardness measurements on each sample as well as the corresponding results of the two groups of experiments.

Table 2
Chemical composition (wt%) of Inconel 625 as confirmed by electron dispersive spectrum (EDS).

Material	Cr	Fe	Ni	Mo	Co	WC
Inconel 625	22.28	2.47	68.08	7.20		

4. Results and discussion

4.1. Development of statistical model

The responses from the experiments were analysed with the mathematical models with best fits determined. The RSM model describes the variation of the measured responses with the independent variables. Analysis of variance (ANOVA) was carried out in stepwise mode in order to eliminate insignificant terms. The detailed process of analysis including ANOVA and other statistics R^2, adjusted R^2, and predicted R^2 were calculated to establish the mathematical models for microhardness, dilution ratio and process efficiency and presented in Tables 4, 5 and 6 respectively.

4.1.1. Microhardness of the laser cladded composite coating

Analysis of variance (ANOVA) was performed for microhardness responses as shown in Table 4. The model *F*-value of 14.69 implies the

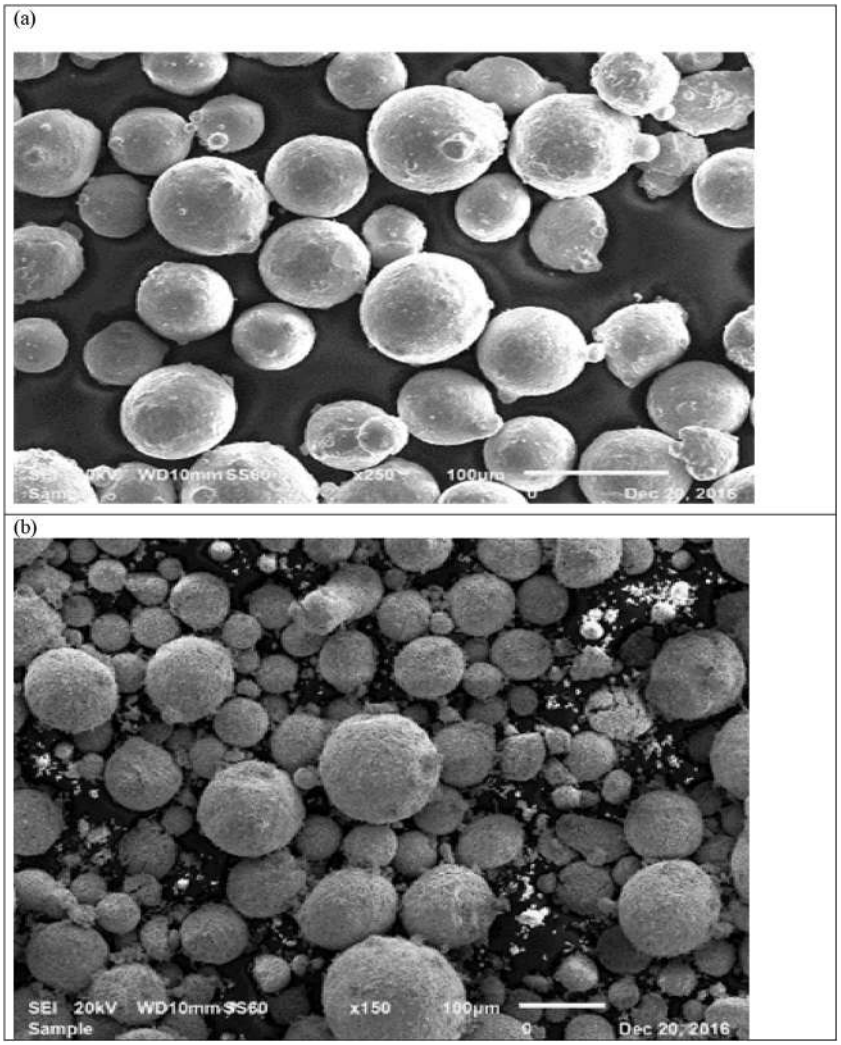

Fig. 2. Scanning electron micrographs (SEM) of (a) as-received Inconel 625 and (b) as-received WC-86 powders.

Fig. 3. The laser system used in depositing the composite coating.

model is significant. A 0.05 p-value suggests that the factor is significant. The only significant model factors for the coatings for microhardness (MH) are energy density (A), inconel content (B) and A^2. Table 4 confirms the larger significant influence of A^2 (F-value = 20.75) in comparison to A (F-value = 10.56) in the impartation of microhardness to the composite coatings. Inconel content has the most significant influence on microhardness with an F-value of 52.47. However, the extent of the effects of energy density (A) and A^2 on the microhardness are significantly lower when compared to the inconel content. R^2 value of 0.8715 obtained for the deposited coatings provides an indication of the nature of co-relation between the experimental data and measured data. The value suggests strong correlation between the predicted and experimental data obtained for microhardness of the coatings. The value obtained for the predicted R^2 of 0.6435 is in reasonable agreement with the adjusted R^2 of 0.8121 (i.e. the difference is < 0.2). Adequate precision measures the signal to noise ratio. Meanwhile, Sun & Hao [22] recommended that a ratio > 4 is desirable, hence, the ratios of 12.9086 obtained in this study indicates an adequate signal. The non-significant value obtained for lack of fit as seen in Table 4 is preferred. Analysis of finding from this study implies that the developed model is suitable for navigating the design space. Therefore, the obtained empirical relationship between the microhardness and the process parameters in terms of coded factors, having eliminated the non-significant terms, is described as follows by Eq. (5) for fiber laser fabricated composite coatings with the standard deviation being ± 13.4% the mean value of microhardness (Table 4):

$$\text{Microhardness} = +652.70125 + 68.05721*A - 151.70422*B - 8.31639*C + 53.46000*AC - 92.42305*A^2 - 20.79666*B^2 \quad (5)$$

Table 3
Central composite design running (experimental results).

Expt. no.	Run order	Cladding parameters			Quality characteristics		
		A	B	C	Micro hardness (M)/HV	Dilution ratio (DR)	Process efficiency (PE) (%)
1	5	13.1	70	4	743.45	0.03	34.42
2	2	21.9	70	4	712.20	0.13	50.00
3	3	13.1	90	4	384.30	0.06	40.63
4	8	21.9	90	4	399.60	0.12	60.33
5	1	13.1	70	12	432.30	0.08	34.71
6	6	21.9	70	12	770.34	0.10	50.43
7	7	13.1	90	12	387.20	0.02	40.38
8	4	21.9	90	12	460.84	0.05	60.34
9	9	10.3	80	8	237.12	0.02	9.05
10	10	24.7	80	8	554.50	0.13	54.87
11	11	17.5	63.7	8	909.20	0.07	42.73
12	12	17.5	96.3	8	287.60	0.03	66.57
13	13	17.5	80	1.47	674.90	0.05	51.26
14	14	17.5	80	14.53	719.70	0.03	51.50
15	15	17.5	80	8	672.30	0.04	51.50
16	16	17.5	80	8	660.60	0.03	46.39
17	17	17.5	80	8	536.50	0.10	43.76
18	18	17.5	80	8	659.80	0.04	51.50
19	19	17.5	80	8	592.00	0.05	44.73
20	20	17.5	80	8	713.30	0.02	54.68

4.1.2. Dilution ratio of the laser cladded composite coating

The model *F*-value of 7.39 (Table 5) suggests that the statistical model for dilution ratio is very significant while p-values < 0.05 imply that the model terms are significant for the coatings. Furthermore, it is preferred that the value of lack of fit is not significant as seen in Table 5. With the adequate precision value of 9.8014 being > 4, it can be inferred the model can be used to navigate the design space. In addition, energy density (A) and the second order of energy density (A^2) are the significant factors which influence the dilution ratio of the composite coating as presented in Table 5. At F-value of 24.62, energy density (A) has greater influence than the second order of energy density (A^2) ($F = 5.58$). R^2 values of 0.7732 depict very strong correlation between the experimental and the predicted values obtained for the dilution ratio of the clads. The value obtained for the predicted R^2 of 0.4975 is in reasonable agreement with the adjusted R^2 of 0.6685 (i.e. the difference is < 0.2). The quadratic mathematical model used to predict the dilution of the composite coatings in terms of coded factors is expressed as follows with the standard deviation being ± 35.8% of the mean value of dilution ratio (Table 5):

$$\text{Dilution ratio} = +0.0509 + 0.0289{*}A - 0.0115{*}B - 0.0091{*}C - 0.0137{*}AC - 0.0163{*}BC + 0.0133{*}A^2 \quad (6)$$

4.1.3. Process efficiency of laser cladded composite coating

Table 6 highlights the ANOVA of the process efficiency (PE) of the coatings as well as the significant model terms determined via stepwise regression method which eliminates the insignificant terms automatically. Again, high F-value (16.32) obtained for the model suggest that it is significant. The implication of the value of the adequate precision (16.6138) being > 4 is that it satisfies the adequate model discrimination. It is preferred that the value (1.10) of lack of fit is not significant as seen in Table 6. Furthermore, the value (0.9223) obtained for R^2 is very close to 1, an indication that the mathematical models developed for process efficiency correlates very strongly with the experimental data. Meanwhile, energy density (A), inconel content (B) and second order of energy density (A^2) are the only significant factors that affect the process efficiency (PE) of coatings as revealed by Table 6. The ultimate empirical model relating to process efficiency, in terms of coded factors is described as follows for the coatings with the standard deviation being ± 9.5% of the mean value of process efficiency (Table 6):

$$\text{Process efficiency} = +49.60 + 10.84{*}A + 5.29{*}B + 0.0662C + 1.04{*}AB + 0.0475AC - 0.1225BC - 5.82{*}A^2 + 2.10{*}B^2 \quad (7)$$

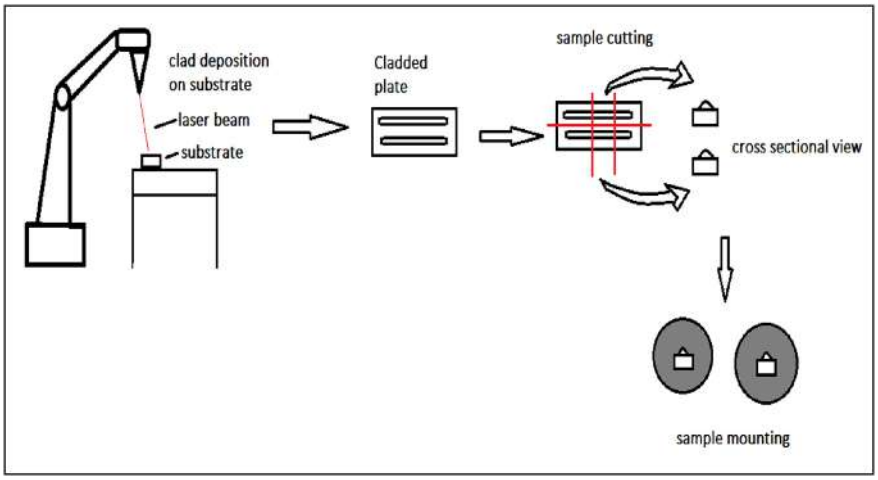

Fig. 4. Schematic diagram of the sample preparation of the laser cladded composite coating.

Table 4
ANOVA for microhardness of the laser cladded composite coating.

Source	Sum of squares	df	Mean squares	F-value	p-Value prob > F
Model	5.280E+05	6	87,994.41	14.69	< 0.0001 Significant
A-Laser energy density	63,255.60	1	63,255.60	10.56	0.0063
B-Inconel content	3.143E+05	1	3.143E+05	52.47	< 0.0001
C-Shielding gas flow rate	944.54	1	944.54	0.1577	0.6977
AC	22,863.77	1	22,863.77	3.82	0.0726
A^2	1.243E+05	1	1.243E+05	20.75	0.0005
B^2	6294.97	1	6294.97	1.05	0.3240
Residual	77,874.09	13	5990.31		
Lack of fit	57,630.30	8	7203.79	1.78	0.2724 Not significant
Pure error	20,243.79	5	4048.76		
Cor total	6.058E+05	19			
Std. dev.	77.40		R^2		0.8715
Mean	575.39		Adjusted R^2		0.8121
C.V. %	13.45		Predicted R^2		0.6435
Press	2.160E+05		Adeq precision		12.9086

Table 5
ANOVA for dilution ratio (DR) of the laser cladded composite coating.

Source	Sum of squares	df	Mean squares	F-value	p-Value prob > F
Model	0.0206	6	0.0034	7.39	0.0013 Significant
A-Energy density	0.0114	1	0.0114	24.62	0.0003
B-Inconel content	0.0018	1	0.0018	3.90	0.0698
C-Gas flow rate	0.0011	1	0.0011	2.41	0.1444
AC	0.0015	1	0.0015	3.26	0.0942
BC	0.0021	1	0.0021	4.55	0.0525
A^2	0.0026	1	0.0026	5.58	0.0345
Residual	0.0060	13	0.0005		
Lack of fit	0.0021	8	0.0003	0.3336	0.9187 Not significant
Pure error	0.0039	5	0.0008		
Cor total	0.0266	19			
Std. dev.	0.0215		R^2		0.7732
Mean	0.0600		Adjusted R^2		0.6685
C.V. %	35.90		Predicted R^2		0.4975
Press	0.0134		Adeq precision		9.8014

4.2. Confirmation of the statistical models

Figs. 5, 6, and 7 further establish that the predictive models described by Eqs. (5), (6) and (7) for microhardness, dilution ratio and process efficiency respectively agree very well with the experimental data for the clads. In addition, three new confirmatory tests were carried out with new independent variables within the range specified in Table 1 in an attempt to validate the adequacy of the models for each response of the coatings. The regression Eqs. (5) to (7) were employed to obtain the predicted responses for microhardness, dilution ratio and process efficiency. Table 7 presents the newly selected independent variables, the measured and predicted responses as well as the percentages of error for the coatings. Finally, Table 7 verifies the adequacy of the models. Meanwhile, comparison of the experimental and predicted values (Table 7) for newly selected independent variables reveals that the predicted values agree well with measured results of the MH, DR and PE models within error margins of +6%, 20% and 20% respectively. Hence, the adequacy of the developed models is verified herein.

Table 6
ANOVA for process efficiency (PE) of the laser cladded composite coating.

Source	Sum of squares	df	Mean squares	F-value	p-Value prob > F
Model	2608.10	8	326.01	16.32	< 0.0001 Significant
A-Laser energy density	1604.74	1	1604.74	80.32	< 0.0001
B-Inconel content	382.06	1	382.06	19.12	0.0011
C-Shielding gas flow rate	0.0598	1	0.0598	0.0030	0.9574
AB	8.69	1	8.69	0.4352	0.5230
AC	0.0181	1	0.0181	0.0009	0.9766
BC	0.1201	1	0.1201	0.0060	0.9396
A^2	510.55	1	510.55	25.55	0.0004
B^2	64.15	1	64.15	3.21	0.1007
Residual	219.78	11	19.98		
Lack of fit	122.86	6	20.48	1.06	0.4862 Not significant
Pure error	96.92	5	19.38		
Cor total	2827.87	19			
Std. dev.	4.47		R^2		0.9223
Mean	46.99		Adjusted R^2		0.8658
C.V. %	9.51		Predicted R^2		0.6697
Press	933.91		Adeq precision		16.6138

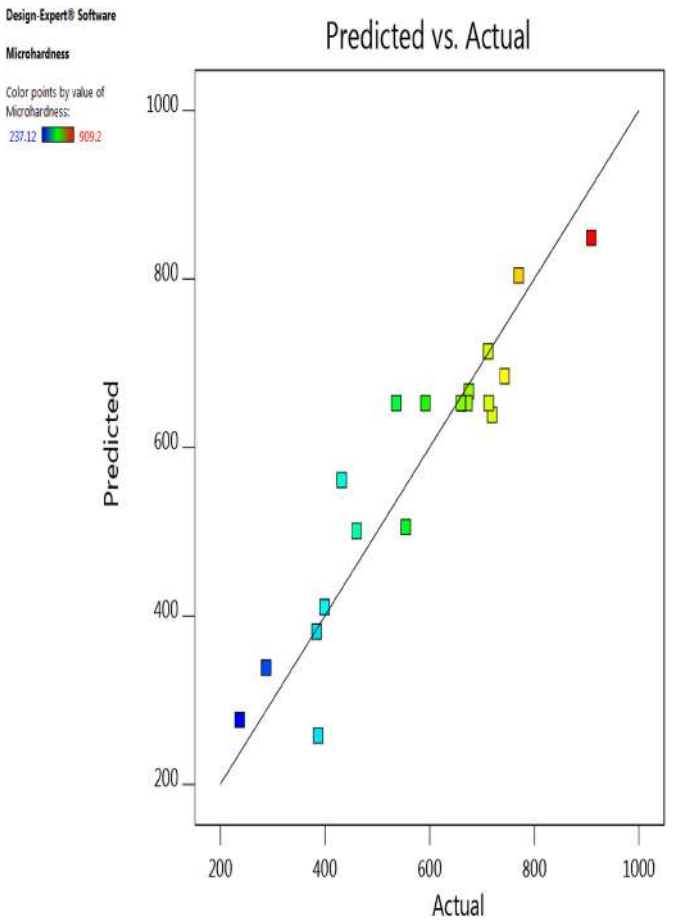

Fig. 5. Predicted vs. measured values of microhardness (*MH*) for fiber laser deposited cladding.

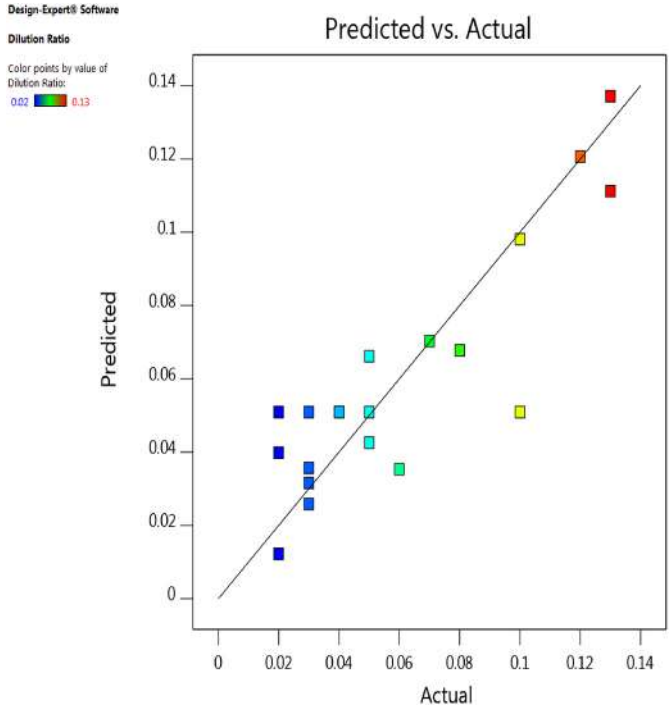

Fig. 6. Predicted vs. measured values of dilution ratio (DR) for fiber laser deposited cladding.

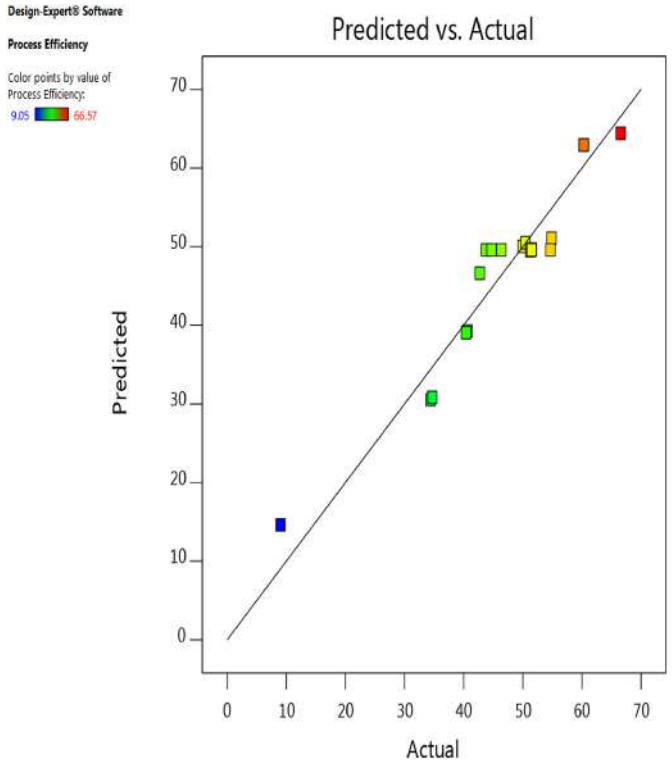

Fig. 7. Predicted vs. measured values of process efficiency (PE) for fiber laser deposited cladding.

4.3. Effects of process parameters on the quality characteristics of the laser cladded composite coatings

4.3.1. Effects of process parameters on the microhardness of the laser cladded composite coating

The perturbation plot presented in Fig. 8 describes how various factors namely: energy density (A), inconel content (B) and gas flow rates (C) influence the microhardness of the composite coatings. This is considered at the centre point of the design space. It is discernible from Fig. 8 that as the laser energy density dissipated into the molten pool increases, the microhardness of the coatings increases to the maximum upon solidification of the melt pool until a certain value of laser energy density (19.7 J/mm^2) is reached. Above this certain value of laser energy density, the microhardness of the coatings is seen to be decreasing. Similar to the findings from tungsten inert gas welding (TIG) of Inconel 825 composite as reported by [26]; it may be inferred that variation in the applied laser energy density induces varying degree of dissolution of the reinforcing WC-86 particles in the melt pool. This fact elucidates varying values of coating's microhardness reported in this study as energy density varies. Analysis of the micrographs of samples fabricated with 80 wt% In and 8 l/min as energy density varies between 10.3 J/mm^2 and 24.7 J/mm^2 also attests to this claim. Although, the temperature of the melt pool was not measured in this study, reported varying degree of dissolution of the reinforcing WC-86 particles in the melt pool which induces different microhardness values in the coatings

Table 7
Confirmatory experiments for the statistical models.

Expt. no.	Energy density (ED)	Inconel content (In)	Gas flow (G)		MH	DR	PE
1	19.7 (0.5)	70.0 (−1)	6.0 (0.5)	Measured	852.59	0.095	59.20
				Predicted	803.74	0.080	49.94
				Error (%)	+6.07	+18.75	+18.54
2	15.3 (−0.5)	80.0 (0)	6.0 (0.5)	Measured	588.56	0.043	49.1
				Predicted	578.04	0.04	42.72
				Error (%)	+1.82	+7.50	+14.93
3	21.9 (1)	90.0 (1)	8.0 (0)	Measured	455.97	0.093	62.30
				Predicted	455.83	0.080	62.95
				Error (%)	0.00	+16.25	−1.03

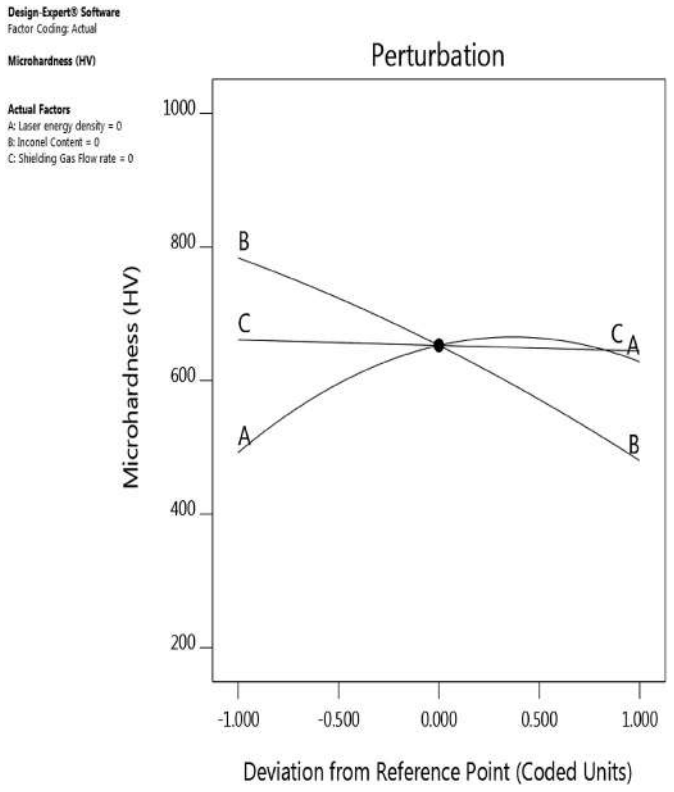

Fig. 8. Perturbation plot showing the effects of all factors on microhardness for composite cladding.

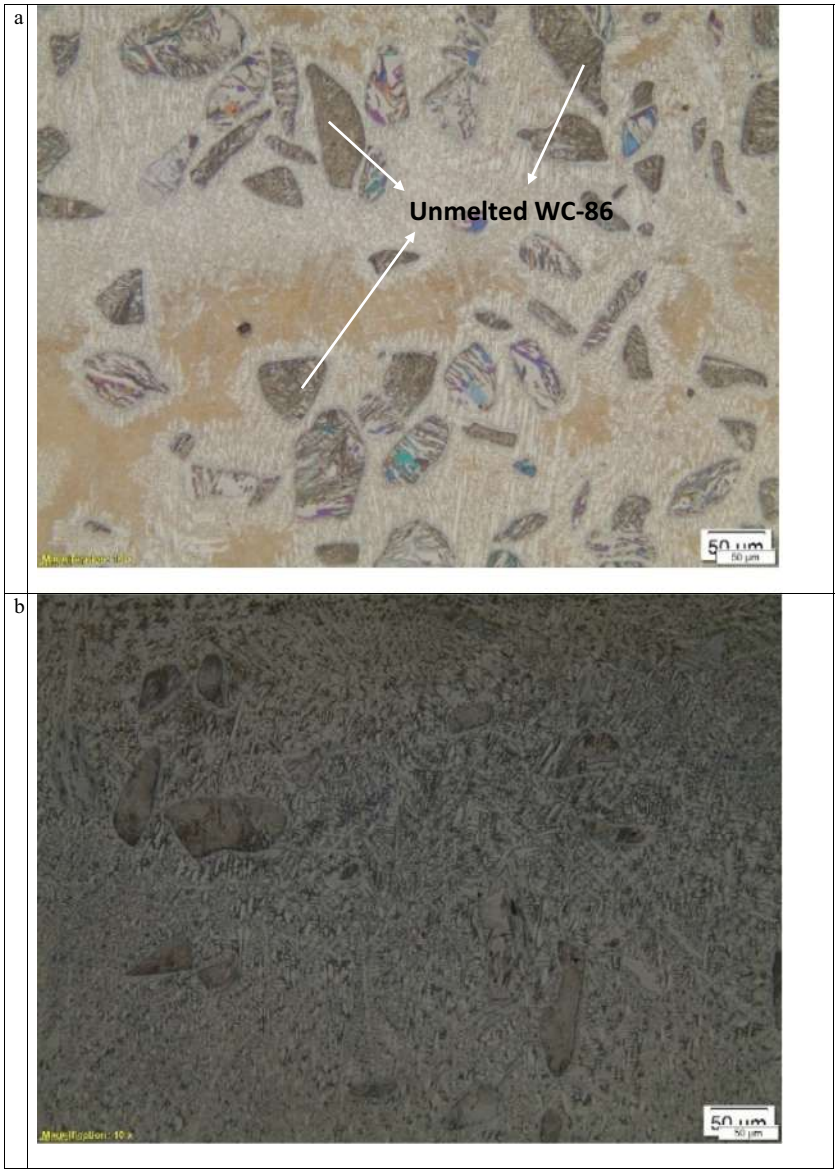

Fig. 9. Optical micrographs showing the effects of energy density (a) 17.5 J/mm^2 and (b) 24.7 J/mm^2, on microstructural evolution of the coatings deposited with 80 wt% In, and 8 l/min.

suggests that variation in energy density induces varying temperature in the melt pool.

Since the deposition for the coating deposited with 10.3 J/mm^2 is very poor such that no observation could be made on the sample, this study will only analyse the micrographs of the composite coatings deposited with 17.5 J/mm^2 and 24.7 J/mm^2 (Fig. 9a, b). It may then be inferred that the available energy density (10.3 J/mm^2) could not melt the blend of powders effectively, hence, the poor deposition to the substrate which accounts for the lowest microhardness reported in this study. Meanwhile, the dissipation of 17.5 J/mm^2 into the molten pool induces a densely and uniformly distributed WC-86 particles within the Inconel 625 matrix (Fig. 9a), hence a relatively higher microhardness it exhibits as seen in Fig. 8 and Table 3. When higher energy density of 24.7 J/mm^2 was employed for processing, it is seen from Fig. 9b that some molten WC-86 particles are nucleated. This evident by the formation of fine dendrite and needle-like phases in the coating's microstructure during solidification of the molten pool as they encounter full melting. As a result, dissolved WC-86 particles diffuse within the molten matrix of Inconel 625. The lower microhardness reported for this processing condition could however be attributed to the molten WC-86 particles reacting with the constituents of the Inconel 625 which might have generated carbides with lower hardness values than those of WC-86 particles [15,23].

Fig. 8 also indicates that Inconel 625 content exerts significant indirect relationship on the microhardness of the composite coatings. Similar to selective laser sintering process [27,28], the consolidation mechanism in laser cladding of Inconel 625/WC-86 composite coating entails incomplete metallurgical melting in which the high melting-point reinforcing WC-86 structural phase is partially melted while the ductile Inconel 625 matrix is fully melted. With the introduction of 96.3 wt% Inconel 625/3.7 wt% WC-86 into the melt pool, the viscosity of the composite melt increases excessively since 3.7 wt% WC-86 might have possibly experienced full melting prompted by its presence in smaller quantity and high surface area to volume ratio. This might have hindered the efficient flow of the pool, and consequently decreasing the overall rheological properties of the melt. Meanwhile, an intensive Marangoni convection which develops within the composite melt also introduces an additional force into the pool [29]. The composite melt containing 96.3 wt% Inconel 625 flows radially inward towards the laser beam centre rather than spreading outward on the underlying

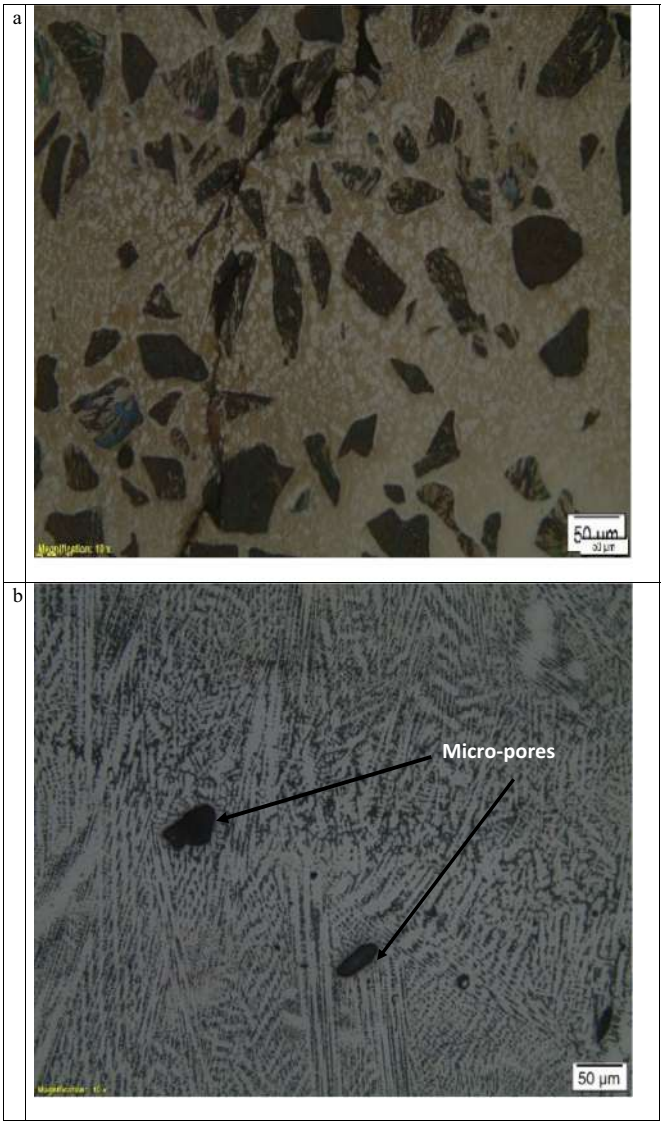

Fig. 10. Optical micrographs showing the effects inconel content on microstructural evolution as well as its dependence on microhardness (a) 17.5 J/mm^2, 63.7 wt% In, and 8 l/min (b) 17.5 J/mm^2, 96.3 wt% In, and 8 l/min.

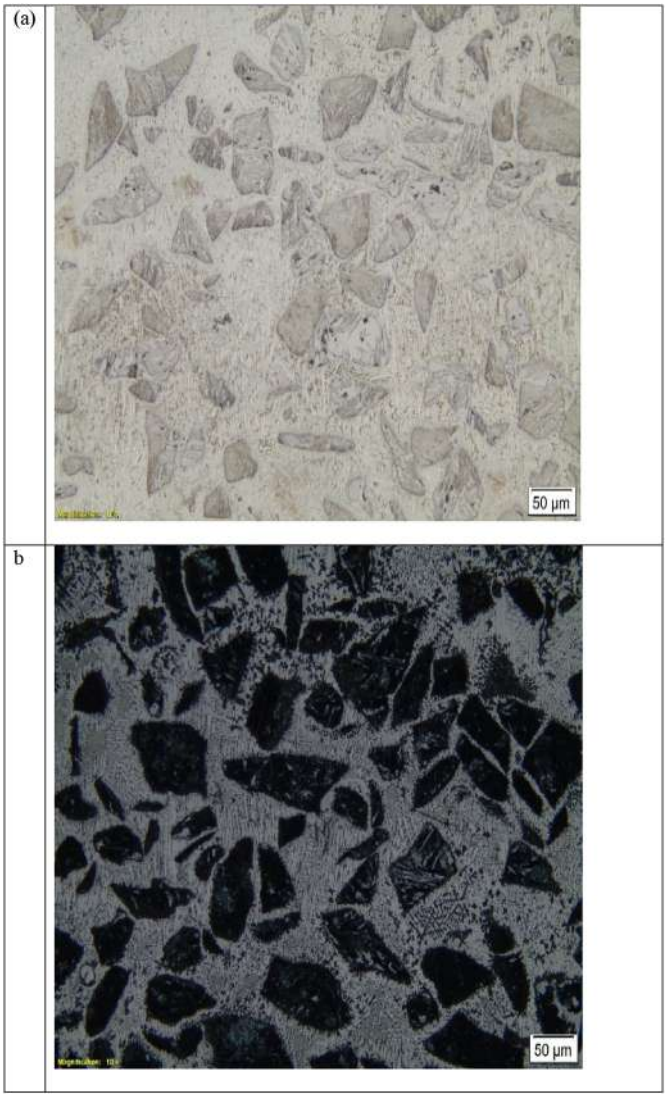

Fig. 11. Optical micrographs showing the effects of gas flow rates on microstructural evolution as well as its dependence on microhardness (a) 13.1 J/mm^2, 70 wt% In, and 4 l/min (b) 13.1 J/mm^2, 70 wt% In, and 12 l/min.

surface due to the synergetic effect of (i) the rheological performance of the melt being handicapped by excessive melt viscosity and (ii) the action of Marangoni force. This imposes adverse consequence on the consolidation mechanism as it takes longer than necessary for the composite melt pool to solidify. This less than desirable densification mechanism could be said to be responsible for micro-porosities which severely degrades the microhardness of the composite coatings (Fig. 10b). At reduced Inconel 625 content (63.7 wt%), the microhardness of the composite coating is seen to be increasing (Table 3). This could be attributed to the reduced melt pool resulting from partial melting of WC-86 rather than its full melting. Therefore, the melt pool is not superheated as the partial melting of WC-86 does not allow for excessive in-situ chemical reactivity of the composite constituents which could have introduced additional thermal energy during laser-material interaction. In this context, the rheology of the melt was not handicapped by excessive melt viscosity and the action of Marangoni force. Consequently, the solidification mechanism of the composite pool occurs within the adequate time required for the formation of pore-free microstructure which ensures increased microhardness of the coatings (Fig. 10a). Meanwhile, Fig. 8 and Table 3 suggest that the shielding gas flow rate has no effect on the microhardness of laser cladded composite coatings as a microhardness was constant irrespective of the rate of gas flow employed during processing. Analysis of the micrographs (Fig. 11a and b) of the coatings fabricated with varying gas flow rates and the same energy density and inconel contents reveals no discernible difference in the microstructure either in terms of the amount of partially or fully melted WC-86 particle, porosities and cracks. Therefore, shielding gas flow rates has no influence on the microhardness of the laser cladded composite coatings. This outcome is corroborated by findings from Chaudhari & More [30] who revealed that shielding gas flow rates has no effect on the microhardness and microstructure of gas metal arc welded (GMAW) 3Cr12 stainless steel.

As seen from Table 4, the interactions between the model terms are quite significant such that they tend to influence the microhardness of the coatings. The interaction between energy density and inconel content as well as energy density and gas flow rates is shown in Fig. 12a and b respectively. With shielding gas flow rate set at zero level, Fig. 12a shows that at inconel content above 85 wt% the microhardness of the composite coatings would be < 400 HV when laser energy density is < 15.3 J/mm^2 is engaged for fabricating the claddings. Between 75 wt% and 85 wt% of inconel content, the microhardness of the coatings is seen to vary between 500 and 700 HV irrespective of the amount of energy density employed during processing.

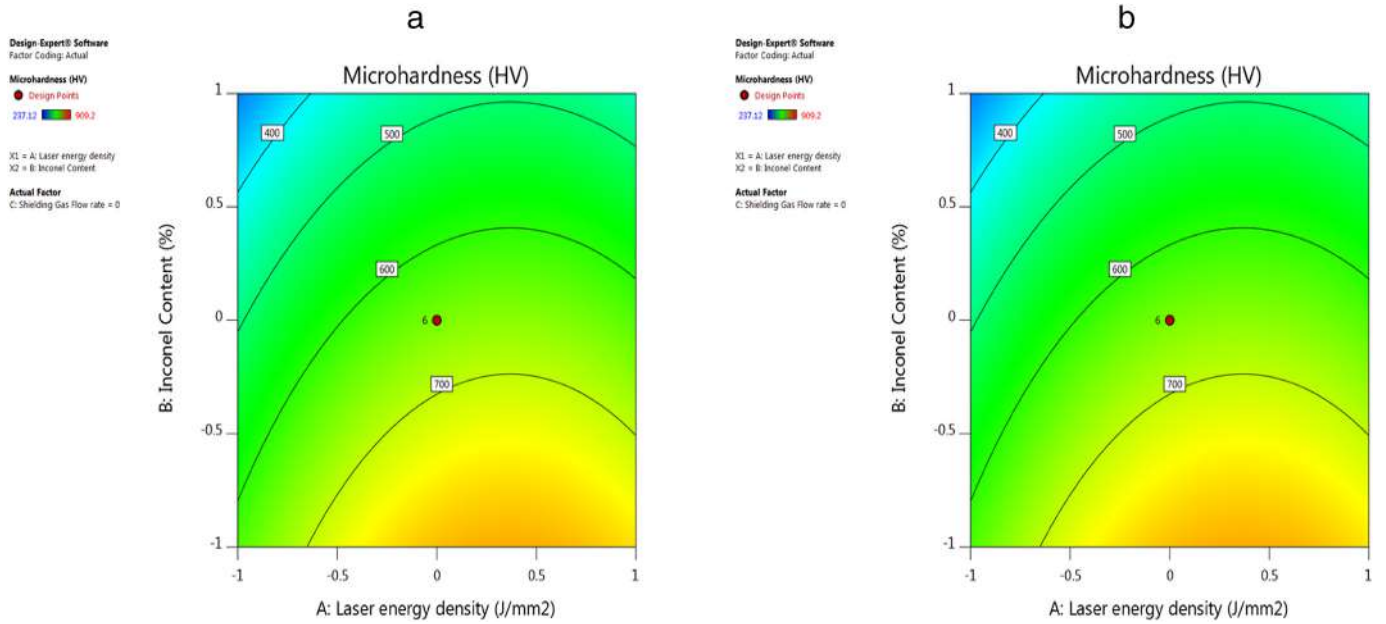

Fig. 12. Contour plots of effects of (a) energy density & inconel content (b) energy density & gas flow rates on microhardness.

Below 75 wt% inconel content, the coating's microhardness would be > 700 HV when energy density is above 15.3 J/mm^2 is dissipated into the materials during processing. Fig. 12b shows that the microhardness of the coatings increases as the laser energy density dissipated during laser-material interaction increases whereas microhardness values are constant as shielding gas is varied for corresponding laser energy density. Comparative analysis of the interactions between inconel content/energy density with that of gas flow rates/energy density reveals that the former has significant influence on the coating's microhardness than the latter. This is evident when considering the range of microhardness values for both Fig. 12a and b. It is discernible that Fig. 12a has a higher range of microhardness (> 300 HV) relative to Fig. 10b (=100 HV).

4.3.2. Effects of process parameters on the dilution ratio of the laser cladded composite coating

Fig. 13 is a perturbation plot which elucidates how laser energy density (A), inconel content (B) and shielding gas flow rates (C) affect the dilution ratio of the deposited coatings. Again, the centre point in the design space is considered in analysing the perturbation plot. It is clear from Fig. 13 that both inconel content and shielding gas flow rates exercise marginal indirect relationship with the dilution ratio (DR). DR highlights the degree of intermixing between the substrate and the coating composite. Reduced dilution ratio noticed at higher values of gas shielding rates could be attributed to its increased cooling effect which minimises the dissipated heat that could have melted more of the substrate. Similar to findings from laser welding and selective laser melting processes [31,32], shielding gas protects the melt pool from chemical reactivity which might lead to generation of additional thermal energy that could result in excessive intermixing of the composite coating and the substrate materials during processing.

Therefore, reduced dilution ratio at higher flow rates of the shielding gas could be ascribed to its minimisation of chemical reactivity that could have generated excessive thermal energy which would have melted both the coatings and the substrate, thereby, increasing dilution ratio. Increased dilution ratio which occurred when lower flow rates of shielding gas was used during processing could be explained by the diminished capability of the shielding gas in protecting the molten pool from chemical reactivity. Hence, increased chemical reactivity at lower flow rates resulted in generating excessive thermal energy which eventually increased the intermixing of the

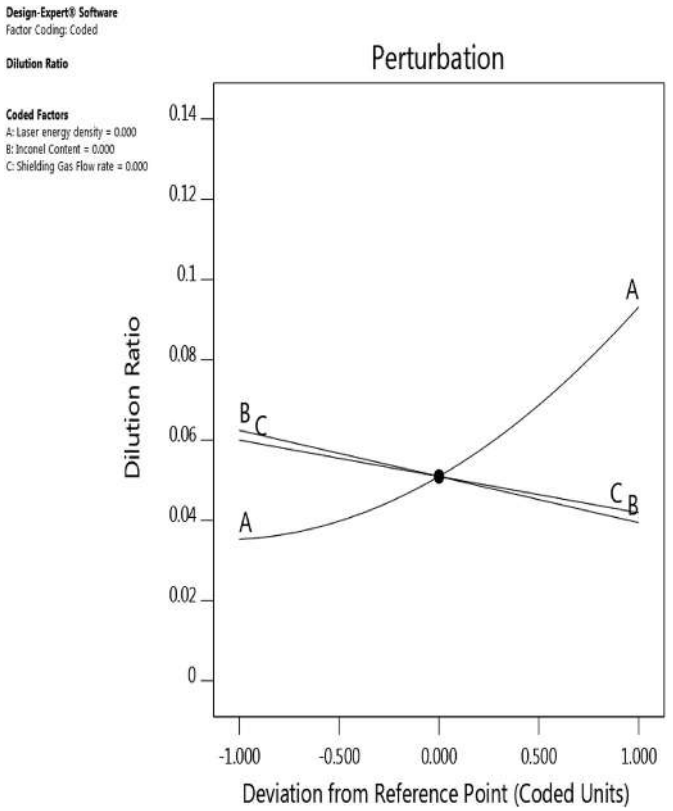

Fig. 13. Perturbation plot showing the effects of all factors on dilution ratio of fiber laser deposited cladding.

coating and substrate materials due to uncontrolled melting. Higher dilution ratio obtained at lower inconel content could be accounted for by the increased WC-86 content which induced chemical reactivity that eventually generated additional thermal energy in the melt pool. It is possible that the additional thermal energy to that of laser energy density could have resulted in increased intermixing of the coating and the substrate materials. At higher inconel content, little or no chemical reactivity occurred as the content of WC-86 had been reduced in the

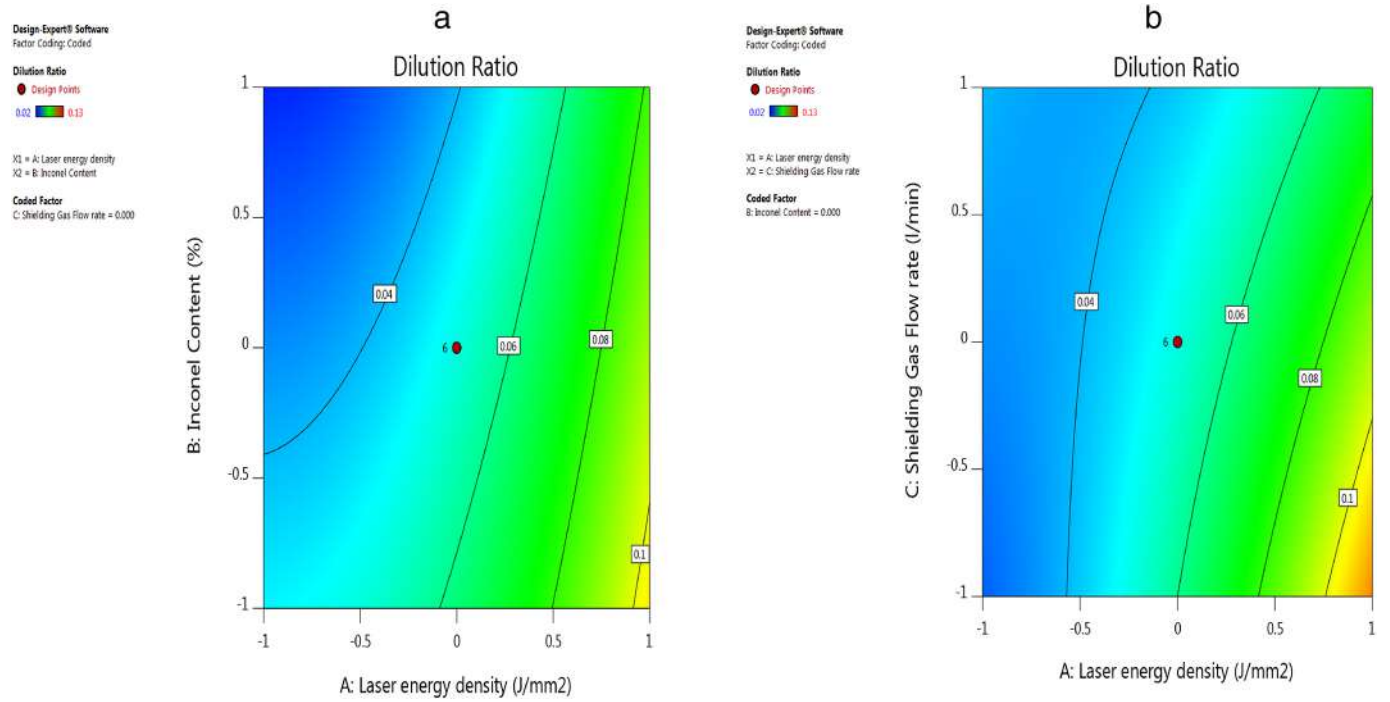

Fig. 14. Contour plots of effects of (a) energy density & inconel content (b) energy density & gas flow rates on dilution ratio.

melt pool. Hence, little or no additional thermal energy is generated, hence, the reduced DR reported at higher inconel content. With the energy density increasing, Fig. 14 reveals that the dilution ratio also increases. As the laser energy density increases, the available thermal energy might be more than what is required to consolidate the available composite powders in depositing the coatings.

Hence, the melt pool of the composite powders might have been superheated as energy density increases. Consequently, the excessive heat which could be not utilised in consolidating its molten pool might have been dissipated into melting the substrate, therefore, the occurrence of the intermixing of the coating and substrate materials which led to increase dilution ratio. Moreover, the dissipation of excessive laser energy into substrate is possible due to the molten pool of the composite coatings taking longer time than necessary to solidify. This might have resulted in increased DR.

Fig. 14a was developed with the inconel content and energy density being varied while the shielding gas flow rates set at zero value. Fig. 14a shows that when laser energy density varying between 13.1 and 17.5 J/mm^2 was employed for depositing the composite coatings, the resultant dilution ratio is 0.04 irrespective of the inconel content utilised during deposition. With the energy density increasing above 17.5 J/mm^2, it is clear from Fig. 14a that the dilution ratio continues to increase independent of the inconel content introduced into the composite coating. Fig. 14b, developed with the inconel content set at zero value, shows that the dilution ratio of the coatings is 0.04 as laser energy density varies between 13.1 and 17.5 J/mm^2 irrespective of the gas flow rates employed during processing. Similar to findings from Fig. 14a, the dilution continues to increase independent of the gas flow rates utilised during processing. Meanwhile, comparative analysis of the influence of the interactions between inconel content/energy density with that of gas flow rates/energy density on the dilution ratio reveals that both are equally influential when their range of values (0.06) is considered (Fig. 14a and b).

4.3.3. Effects of process parameters on the process efficiency of the laser cladded composite coating

Fig. 15 shows the effects of energy density, inconel content and shielding gas flow rates on the process efficiency of laser cladded

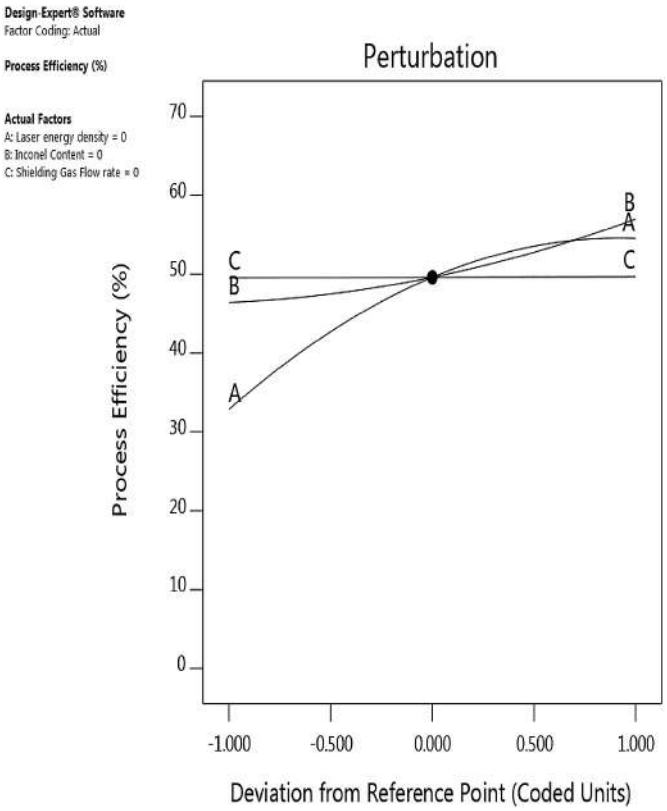

Fig. 15. Perturbation plot showing the effects of all factors on process efficiency for fiber laser deposited cladding.

Inconel 625/WC-86 composite coating. It is clear from Fig. 15 that the process efficiency continues to increase up to a maximum value of 52.5% as the laser energy density increases up to 19.70 J/mm^2. Further increase in laser energy density beyond 19.70 J/mm^2 does not lead to improvement in process efficiency as seen in Fig. 15. The composite

powders have to be melted by the laser energy density being dissipated and powdered particles should not rebound away from the substrate's surface provided the optimum process efficiency has not been attained. Therefore, increased process efficiency noted as energy density increases from 13.10 to 19.70 J/mm^2 could be attributed to the capacity of the melted pool to embed more particles. The embedded composite particles then become plastic and eventually melted and deposited due to thermal energy being transferred from the pool. Consequently, the particles are deposited without rebounding after staying in contact with the surface for a long time.

The stagnation in the process efficiency as laser energy density is increased above 19.70 J/mm^2 could be linked to the possibility that the capacity of the molten pool to absorb more composite particles had reached the saturation state. Therefore, the molten pool at the surface had already encountered rapid solidification such that additional particles being introduced are then rebounded away. This observation is similar to that reported by Simchi and Pohl [33] in their work elucidating the effects of laser sintering processing parameters on the microstructure and densification of iron powder. The additional thermal energy being dissipated into the solidified coating is then transferred into the substrate. It is this which causes the intermixing of the coating and substrate materials which results in increased dilution ratio. The implication of this finding is that the optimum energy density that can be used in depositing Inconel 625/WC-86 composite is 19.70 J/mm^2 if wastage of materials and laser energy as well as intermixing of the coating and substrate materials are to be avoided. It is clear from Fig. 15 that the process efficiency remains constant as shielding gas flow rates increase whereas the process efficiency increases marginally as inconel content increases. Marginal increase reported in process efficiency as inconel content increases could be ascribed to the fact inconel particles have lower melting point and higher density (8.44 g/cm^3) in comparison to WC-86 which is characterised with higher melting point and lower density (4.3 g/cm^3). These physical properties of Inconel 625 favours increased deposition efficiency as its content increases within the composite coating. Further studies will be needed to explore the explanation for constant values of process efficiency obtained as the shielding gas flow rates increases.

Fig. 16a was developed with the inconel content and energy density being varied while the shielding gas flow rates set at zero value. Fig. 16a further shows that the laser energy density has significant influence on the process efficiency with inconel content exercising marginal increase as laser energy density varies. Therefore, the process efficiency is optimised when laser energy density > 17.5 J/mm^2 is adopted for processing. Fig. 16b, developed with the inconel content set at zero value, also reveals that the process efficiency increases as laser energy density increases irrespective of the gas flow rates employed during processing. Comparative analysis of the influence of the interactions between inconel content/energy density with that of gas flow rates/energy density on the process efficiency reveals that the former is more influential than the latter when their range of values are considered (Fig. 16a and b).

4.4. Optimisation and confirmation

A composite coating with high hardness and minimum dilution ratio is desired to avoid customer's rejection. Moreover, it is anticipated that high quality coatings be deposited at high process efficiency such that materials' wastage is minimised so that manufacturers can make profits. Therefore, the need to determine appropriate interaction between the independent parameters which ensures the deposition of high quality coatings such that manufacturers can sustain the production process. A critical consideration of findings from this study indicates that the selection of parameters for enhancing coatings' microhardness tends to oppose that of dilution ratio while the need to maximise process efficiency demands that selected parameters must balance the competing interests of microhardness and dilution ratio. For instance, increasing the microhardness of the coatings necessitates that less of Inconel 625 needs to be introduced into the composite coating when employing higher laser energy density for fabricating the claddings while the contrary is true for dilution ratio which needs to be minimised by employing lower laser energy density (see Figs. 12, 14 and 16). Therefore, these criteria guided the selection of optimised quality parameters. The desirability function [34] for multiple responses described in Eq. (8) enables all independent variables to be optimised simultaneously.

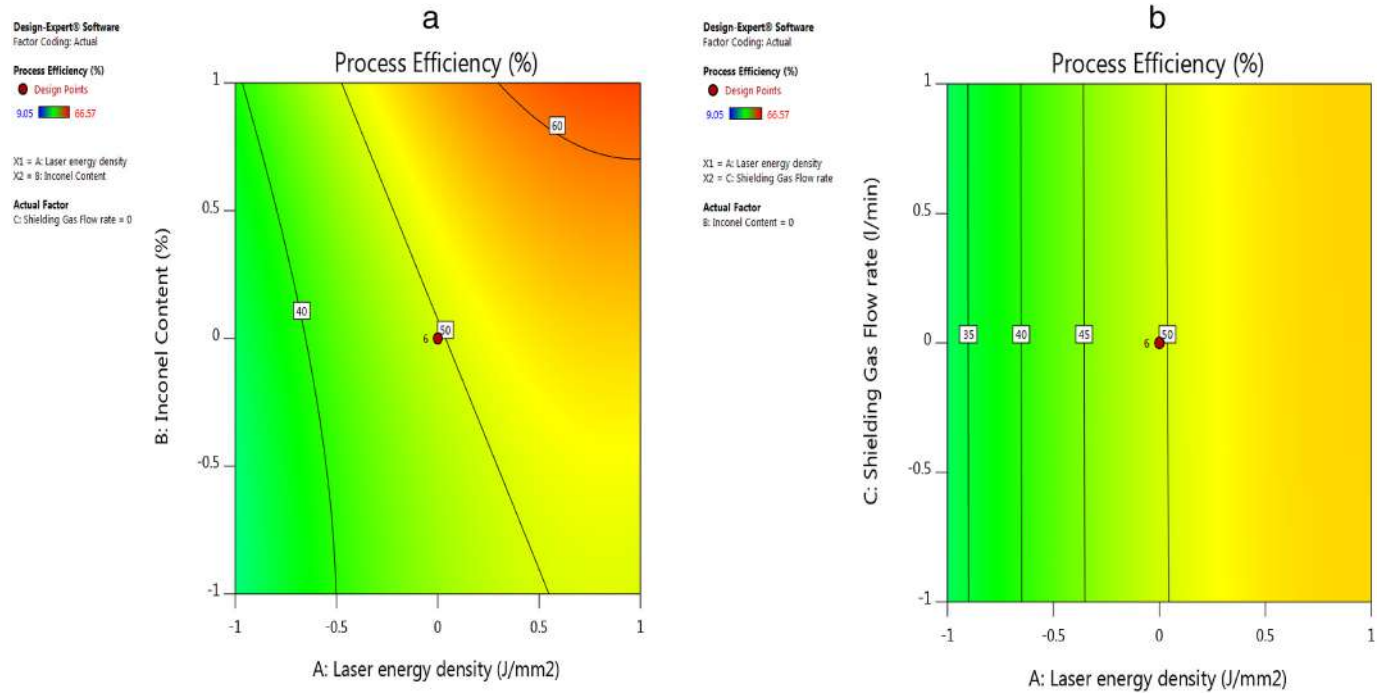

Fig. 16. Contour plots of effects of (a) energy density & inconel content (b) energy density & gas flow rates on process efficiency on Fiber laser deposited cladding.

Table 8
Numerical optimisation for central composite design.

Expt. no.	Energy density (ED)	Inconel content (In)	Gas flow rate (G)	MH (V)	DR	PE (%)	Desirability	
1[a]	0.254	−0.237	0.216	700.00	0.060	50.00	1.000	Selected
2	0.255	−0.237	0.208	700.0	0.060	50.00	1.000	
3	0.240	−0.202	0.106	694.00	0.060	50.00	0.996	
4	0.248	−0.236	0.289	700.00	0.059	50.00	0.993	
5	0.123	−0.272	−0.343	700.00	0.060	48.77	0.990	
6	0.029	−0.264	−1.000	700.00	0.060	48.75	0.990	
7	0.097	−0.274	−0.505	700.00	0.060	48.64	0.989	
8	0.094	−0.274	−0.525	700.00	0.060	48.63	0.989	
9	0.055	−0.271	−0.799	700.00	0.060	48.62	0.989	
10	0.057	−0.271	−0.783	700.00	0.060	48.62	0.989	
11	0.066	−0.272	−0.719	700.00	0.060	48.60	0.988	
12	0.068	−0.273	−0.700	700.00	0.060	48.60	0.988	
13	0.075	−0.273	−0.654	700.00	0.060	48.60	0.988	
14	−0.330	−0.781	1.000	700.00	0.060	43.21	0.941	
15	−0.358	−0.809	0.932	700.00	0.060	42.63	0.936	

[a] Selected.

$$\left[\prod_{i=1}^{N} d_i^{r_i}\right]^{1/\sum r_i} \quad (8)$$

N = Number of responses
r_i = The importance of some particular response
d_i = The partial desirability function for specific responses.

In regard to laser cladding of composite coatings, desirability function is implemented by assigning desirable high or low limit specifications to each output variable/response. Thereafter, a search for optimum experimental condition with the range of process of parameters employed in this study is carried out with a view to optimising coatings' microhardness (≥700 HV) and process efficiency (≥50%) while minimising the dilution ratio (≤0.06). Design Expert statistical software was employed to explore the optimum experimental conditions for achieving the desirable quality characteristics of the composite coatings. The rationale for this optimisation goal is to ensure that not more than half of composite materials are lost during deposition while ensuring sufficiently hard coatings with minimal dilution ratio. The most desirable operating conditions are presented in Table 8. In addition, process economics also demand that consideration is given to the cost of purchasing shielding gas, Inconel 625 content and laser energy density (in the increasing order of importance) when selecting the most desirable operating conditions for producing the optimum composite coatings. Therefore, it is desired that optimum composite coatings are produced with minimum laser energy density which cost least in comparison to the cost of Inconel 625 and shielding gas. Hence, it is discernible from Table 8 that the most desirable operating conditions are energy density = 18.6 J/mm^2; inconel content = 67.6 wt%; and shielding gas flow rates = 8.86 l/min. This optimum operating condition has a desirability value of 1.00 with optimising coatings' microhardness > 700 HV; process efficiency = 50% and dilution ratio = 0.06. A confirmatory experiment was conducted to validate the optimal process parameters established by CCD. Experimental outcomes, shown in Table 9, reveal that composite coatings with the desired specifications can be deposited by employing the optimal process parameters. The measured results are found to in good agreement with predicted results and the error range between them falls within +3 to 20%. Fig. 17 shows the composite coating obtained by the selected optimum parameters. The coating is characterised with coherently bonded substrate-coating interface devoid of defects such as porosities and crack (Fig. 17a) while the microstructure is imparted with densely and uniformly distributed WC-86 particles within the Inconel 625 matrix (Fig. 17b).

Table 9
Comparative analysis of the experimental and predicted outcomes by employing the optimal experimental conditions.

	Microhardness (HV)	Dilution ratio	Process efficiency (%)
Experimental	726.07	0.07	60.0
Predicted	700.0	0.06	50.0
Error (%)	+ 3.71	+16.67	+20.00

5. Conclusions

This study employs RSM in order to optimise the quality characteristics of laser cladded Inconel 625/WC-86 composite coatings deposited on 304L stainless steel substrate. The following can be inferred from this study by considering the range of process parameters adopted in this study:

- Analysis of variance (ANOVA) indicates that laser energy density and Inconel content have significant influence on microhardness and process efficiency while only energy density significantly influences dilution ratio of the laser deposited Inconel 625/WC-86 composite clads.
- Microhardness increases with laser energy density up to a threshold of 19.7 J/mm^2 (0.5 coded unit). Further increase in energy density above the threshold value results in reduction in microhardness of the coatings. Also, dilution ratio increases with laser energy density. Consequently, the process efficiency increases with increase of laser energy up to an optimum of 19.70 J/mm^2. Increase in laser energy density above 19.70 J/mm^2 yields no increase in process efficiency as the additional thermal energy is dissipated into the substrate where it causes its intermixing with the coating materials.
- Inconel 625 content has an indirect relationship with microhardness and dilution ratio while it has no effect on process efficiency.
- The flow rates of shielding/carrier gas have no effect on microhardness and process efficiency whereas it has an indirect relationship with the dilution ratio.
- Desirability value of 1.00 yielded the most desirable processing conditions which are energy density = 18.60 J/mm^2; inconel content = 67.60 wt%; and shielding gas flow rates = 8.86 l/min. This optimum operating condition produced coatings with microhardness = 726 HV; process efficiency = 60% and dilution ratio = 0.07. The RSM mathematical model is found to predict the quality characteristics of the coatings within the error of 20%.

Finally, the developed RSM mathematical models are reliable and adequate in predicting the quality characteristics of the laser deposited

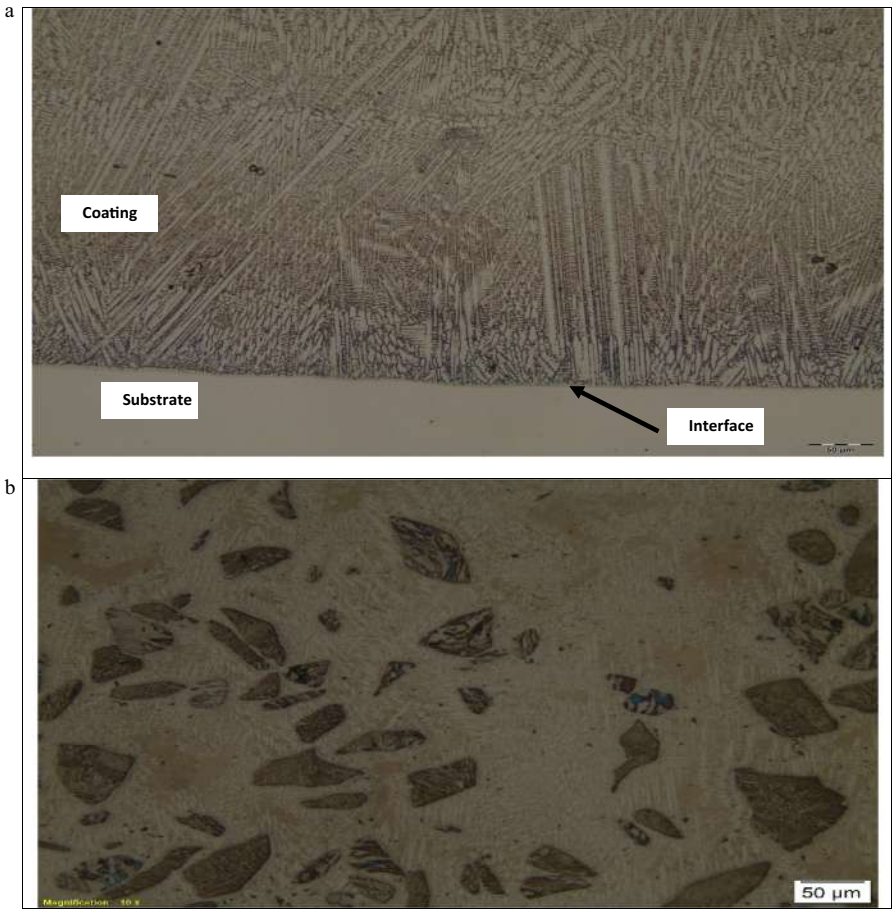

Fig. 17. Micrographs of the optimum sample showing (a) the coherent adhesion between the composite coating and the 304L stainless steel substrate and (b) the uniform distribution of the WC within the Inconel 625 matrix.

coatings and process for mass production. This ensures that the quality characteristics of the coatings and process can be tailored towards meeting the specifications so as to ensure judicious use of materials and energy.

Acknowledgments

This research is supported by the African Laser Center (ALC) under Grant no. CSIR-NLC Reference LHIL 500 task ALC R008 & R010 and Botswana International University of Science & Technology (BIUST) Research Initiation Fund under Grant no. BIUST/ds/r&I/7/2016. The authors are grateful to Mr. Samuel Skhosana for his assistance in operating the laser facility at CSIR.

References

[1] D. Janicki, Laser cladding of Inconel 625-based composite coatings reinforced by porous chromium carbide particles, Opt. Laser Technol. 94 (2017) 6–14.
[2] C. Chang, D. Verdi, M.A. Garrido, J. Ruiz-Hervias, Micro-scale mechanical characterization of Inconel cermet coatings deposited by laser cladding, Boletin de La Sociedad Espanola de Ceramica Y Vidrio 55 (4) (2016) 136–142.
[3] D.E. Cooper, N. Blundell, S. Maggs, G.J. Gibbons, Additive layer manufacture of Inconel 625 metal matrix composites, reinforcement material evaluation, J. Mater. Process. Technol. 213 (12) (2013) 2191–2200.
[4] L. St-Georges, Development and characterization of composite Ni–Cr + WC laser cladding, Wear 263 (1–6) (2007) 562–566.
[5] D. Jiang, C. Hong, M. Zhong, M. Alkhayat, A. Weisheit, A. Gasser, H. Zhang, I. Kelbassa, R. Poprawe, Fabrication of nano-TiCp reinforced Inconel 625 composite coatings by partial dissolution of micro-TiCp through laser cladding energy input control, Surf. Coat. Technol. 249 (2014) 125–131.
[6] J.T. Hofman, D.F. deLange, B. Pathiraj, J. Meijer, FEM modelling and experimental verification for dilution control in laser cladding, J. Mater. Process. Technol. 211 (2011) 187–196.
[7] Q.Y. Wang, S.L. Bai, Z.D. Liu, Corrosion behaviour of HastelloyC22 coating produced by laser cladding in static and cavitation acid solution, Trans. Nonferrous Metals Soc. China 24 (2014) 1610–1619.
[8] Q. Li, Y. Lei, H. Fu, Laser cladding in-situ NbC particle reinforced Fe-based composite coatings with rare earth oxide addition, Surf. Coat. Technol. 239 (2014) 102–107.
[9] J. Tuominen, P. Vuoristo, T. Mantyla, J. Latokartano, J. Vihinen, P.H. Andersson, Microstructure and corrosion behaviour of high power diode laser deposited Inconel 625 coatings, J. Laser Appl. 15 (2003) 55, https://doi.org/10.2351/1.1536652.
[10] L. Sexton, S. Lavin, G. Byrne, A. Kennedy, Laser cladding of aerospace materials, J. Mater. Process. Technol. 122 (2002) 63–68.
[11] T.E. Abioye, D.G. Mccartney, A.T. Clare, Laser cladding of Inconel 625 wire for corrosion protection, J. Mater. Process. Technol. 217 (2015) 232–240.
[12] D. Verdi, M.A. Garrido, C.J. Múnez, P. Poza, Mechanical properties of Inconel 625 laser cladded coatings: depth sensing indentation analysis, Mater. Sci. Eng. A 598 (2014) 15–21.
[13] S. Singh, A.S. Shahi, Metallurgical, wear and fatigue performance of Inconel 625 weld claddings, J. Mater. Process. Technol. 233 (2016) 1–8.
[14] X. Xu, G. Mi, L. Chen, L. Xiong, P. Jiang, X. Shao, C. Wang, Research on microstructures and properties of Inconel 625 coatings obtained by laser cladding with wire, J. Alloys Compd. 715 (2017) 362–373.
[15] T.E. Abioye, P.K. Farayibi, D.G. McCartney, A.T. Clare, Effect of carbide dissolution on the corrosion performance of tungsten carbide reinforced Inconel 625 wire laser coating, J. Mater. Process. Technol. 231 (2016) 89–99.
[16] K.Y. Benyounis, A.G. Olabi, Optimization of different welding processes using statistical and numerical approaches — a reference guide, Adv. Eng. Softw. 39 (6) (2008) 483–496.
[17] K.Y. Benyounis, A.G. Olabi, M.S.J. Hashmi, Effect of laser welding parameters on the heat input and weld-bead profile, J. Mater. Process. Technol. 164–165 (2005) 978–985.
[18] K.Y. Benyounis, A.G. Olabi, M.S.J. Hashmi, Optimizing the laser-welded butt joints of medium carbon steel using RSM, J. Mater. Process. Technol. 164–165 (2005) 986–989.
[19] A.R. Hamad, J.H. Abboud, F.M. Shuaeib, K.Y. Benyounis, Surface hardening of commercially pure titanium by laser nitriding: response surface analysis, Adv. Eng. Softw. 41 (4) (2010) 674–679.
[20] A. Soveja, E. Cicală, D. Grevey, J.M. Jouvard, Optimisation of TA6V alloy surface

laser texturing using an experimental design approach, Opt. Lasers Eng. 46 (9) (2008) 671–678.
[21] H.A. Eltawahni, A.G. Olabi, K.Y. Benyounis, Investigating the CO_2 laser cutting parameters of MDF wood composite material, Opt. Laser Technol. 43 (3) (2011) 648–659.
[22] Y. Sun, M. Hao, Statistical analysis and optimization of process parameters in Ti6Al4V laser cladding using Nd:YAG laser, Opt. Lasers Eng. 50 (7) (2012) 985–995.
[23] T.E. Abioye, Laser Deposition of Inconel 625/Tungsten Carbide Composite Coatings by Powder and Wire Feedstock, Department of Mechanical, Materials and Manufacturing Engineering, The University of Nottingham, 2014 (PhD Thesis).
[24] H.K. Lee, Effects of the cladding parameters on the deposition efficiency in pulsed Nd:YAG laser cladding, J. Mater. Process. Technol. 202 (2008) 321–327.
[25] E.O. Olakanmi, Optimization of the quality characteristics of laser-assisted cold-sprayed (LACS) aluminum coatings with Taguchi design of experiments (DOE), Mater. Manuf. Process. 31 (11) (2016) 1490–1499.
[26] S. Saroj, C.K. Sahoo, M. Masanta, Microstructure and mechanical performance of TiC-Inconel825 *composite* coating deposited on AISI 304 steel by TIG *cladding* process, J. Mater. Process. Technol. 249 (2017) 490–501.
[27] E.O. Olakanmi, R.F. Cochrane, K.W. Dalgarno, Densification mechanism and microstructural evolution in selective laser sintering of Al-12Si powders, J. Mater. Process. Technol. 211 (1) (2011) 113–121.
[28] E.O. Olakanmi, R.F. Cochrane, K.W. Dalgarno, A review on selective laser sintering/melting (SLS/SLM) of aluminium alloy powders: processing, microstructure, and properties, Prog. Mater. Sci. 74 (2015) 401–477.
[29] D. Gu, G. Meng, C. Li, W. Meiners, R. Poprawe, Selective laser melting of TiC/Ti bulk nanocomposites: influence of nanoscale reinforcement, Scr. Mater. 67 (2012) 185–188.
[30] P.D. Chaudhari, N.N. More, Effects of welding process parameters on microhardness and microstructure, Int. J. Eng. Res. Technol. 3 (5) (2014) 1937–1942.
[31] W.M. Steen, J. Mazumder, Laser Material Processing, fourth ed., Springer, London, 2010.
[32] B. Ferrar, L. Mullen, E. Jones, R. Stamp, C.J. Sutcliffe, Gas flow effects on selective laser melting (SLM) manufacturing performance, J. Mater. Process. Technol. 212 (2012) 355–364.
[33] A. Simchi, H. Pohl, Effect of laser sintering processing parameters on the microstructure and densification of iron powder, Mater. Sci. Eng. A 359 (1–2) (2003) 119–128.
[34] D.C. Montgomery (Ed.), Design and Analysis of Experiments. International Student Version, eight ed., John Wiley & Sons, Singapore, 2013.